CXMS and XRD analyses of heat treated A533B stainless steel

E. Morelos-López · A. Cabral-Prieto · N. Nava ·
F. García-Santibañez · C. Nosetti

Abstract Heat induced surface changes on A533B stainless steel were followed by XRD and CXMS techniques. Whereas the XRD patterns of the studied A533B samples were characteristic of α-Fe phase only, the surface Mössbauer spectrum showed a broad sextet, being fitted with two magnetic patterns whose hyperfine magnetic fields were 33 and 31 T associated with a pure and perturbed α-Fe phase, respectively and a broad singlet with an isomer shift $\delta_{A533B} = -0.115(4)$ mms^{-1}/α-Fe, characteristic of the γ-Fe phase. This singlet, probably, arising from the samples' surface only was further analyzed by using a singlet and a quadrupole doublet. From hyperfine distribution and discrete value calculations of their corresponding hyperfine parameters, the quadrupole interaction was the most affected by thermal treatments ranging from 300° to 700 °C showing a slight decrease at 600 °C. The average values of the hyperfine parameters were $\delta_1 = -0.110(6)$ mms^{-1}/α-Fe for the

E. Morelos-López · F. García-Santibañez · C. Nosetti
Laboratorio de Física de Materiales, Facultad de Ciencias, Universidad Autónoma del Estado de México, El Cerrillo Piedras Blancas, Toluca, Estado de México, México

E. Morelos-López
e-mail: lme892@gmail.com.mx

F. García-Santibañez
e-mail: fegasa@uamex.mx

C. Nosetti
e-mail: fegasa@uamex.mx

A. Cabral-Prieto (✉)
Laboratorio de Química, Instituto Nacional de Investigaciones Nucleares, Apdo. Postal 18-1027, Col. Escandón, Del. M. Hidalgo, C. P. 11801, México, D. F. México
e-mail: agustin.cabral@inin.gob.mx

N. Nava
Departamento de Caracterización, Instituto Mexicano del Petróleo, Eje Central Lázaro Cárdenas 152, Col. San Bartolo Atepehuacan, Del. Gustavo A. madero, C. P. 07730 México, D. F. México
e-mail: Noel@imp.mx

Published online: 24 January 2014

꧁ Springer

singlet, and $\delta_2 = -0.081$ (6) mms^{-1}/α-Fe and $\Delta_2 = 0.143(7)$ mm/s) for the quadrupole doublet, respectively. In spite of the temperature dependence of the quadrupole splitting on the doublet, which was higher than that of the isomer shifts of both patterns, only a single defect type was suggested, being associated with monovacancias near the ^{57}Fe sites.

Keywords Mössbauer spectroscopy · Stainless steels · Metallic defects · Hyperfine distributions

1 Introduction

Stainless steels used in the nuclear industry are generally subject to high doses of radiation in such a way that their useful lifetime in a nuclear reactor is shortened, mainly due to a large amount of micro structural defects generated by radiation effects [1]. Microstructure changes in the bulk and surface of these steels are produced by the interaction between neutrons and atoms. Neutrons interact with atoms in a material only when they collide with a nucleus; γ-rays also interact with atoms by photoelectric and Compton interactions. Since neutrons are not attracted or deviated by ions, as occurs to α or β particles, they can travel through the material over relatively large distances before one of them collides with a nucleus which may be displaced from its equilibrium position, thus generating vacancies and interstitials. Many collisions can occur, however, before the energy of the neutrons is slowed down and finally captured by a nucleus. Such a nucleus becomes radioactive and a nuclear decay process starts that may generate new point defects in the material. Vacancies, interstitials or point defect clustering can occur by additional thermal differences in these stainless steels, modifying finally the original mechanical properties of these nuclear materials. Thermal treatments alone can also modify the mechanical properties paralleling those produced by radiation damages [2]. Thus by these thermal treatments it is possible to analyze a variety of physical properties of these nuclear steels.

In this context the aim of this paper was to analyze the surface changes produced by thermal effects on A533B stainless steel by using surface Mössbauer spectroscopy (CXMS) and X-ray diffraction (XRD).

2 Experimental

Several A533B stainless steel samples with $1.0 \times 0.5 \times 0.2$ cm dimensions were used in this study. The elemental composition of this steel was C(0.19), Si (0.25), Mn (1.14), Cr (0.12) Ni (0.84), Mo (0.5), V (0.003), S (0.004), P(0.017), Cu (0.14). The samples were initially put inside quartz tubes under high vacuum (10^{-06} torr), followed next by (a) a heat treatment at 1000 °C in an electric furnace for 30 min and subsequently quenched in water at room temperature; then (b) these samples were reheated by pairs at 300 °C, 400 °C, 500 °C, 600 °C and 700 °C in the electric furnace for 30 min under atmospheric conditions and slowly air cooled at room temperature [2]. The surface analysis was carried out by using Conversion X-rays Mössbauer spectroscopy (CXMS) and X-ray diffraction (XRD). A Mössbauer system operating in the constant acceleration mode with a ^{57}Co/Rh source was used to record the Mössbauer spectra at room temperature. The low gas flux proportional detector, consisting of a gas mixture of Ar + 10 %V CH$_4$ [3] was used to register the conversion X-rays; the reported isomer shifts are referred to that of α-Fe. The
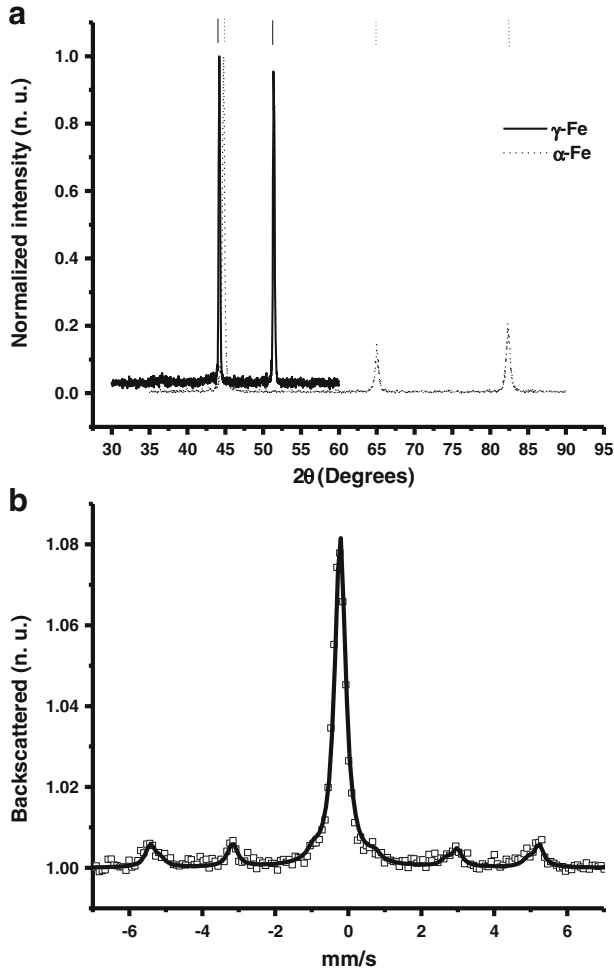
Fig. 1 **a** Characteristic XRD patterns of the A533B and the austenitic AISI 316 stainless steel samples, and **b** characteristic CXMS spectrum of the untreated and treated A533B stainless steel samples

XRD patterns were recorded by using the D5000 diffractometer coupled to a CuKα X-ray source from Siemens.

3 Results

3.1 XRD data

The XRD pattern of the untreated and heat treated A533B samples, recorded from 35° to 90° (2θ), showed the presence of the α-Fe phase only, as shown in Fig. 1a. For a proper discussion of the Mössbauer results, the XRD pattern of AISI-316 stainless steel used as a reference material in Mössbauer spectroscopy and recorded from 35° to 65° (2θ) only is also shown in Fig. 1a. The XRD pattern of this reference material is characteristic of the

γ-Fe phase and was not observed in the XRD pattern of any of the A533B stainless steel samples. Each pattern in Fig. 1a is identified according to the metal phase.

3.2 Mössbauer data

3.2.1 Surface Mössbauer spectra of the A533B stainless steel

The CXMS spectrum of any A533B sample (untreated or heat treated) showed superimposed broad Mössbauer spectra, composed of a sextet and a singlet, as shown in Fig. 1b. The hyperfine parameters of these patterns are: $\delta_m = 0.003(1)$ mms^{-1}/α-Fe, $\Delta_m = 0.009(2)$, $B_m = 32.87(9)$ T for the sextet and $\delta_s = -0.115(1)$ mms^{-1}/α-Fe for the singlet. The line widths are $W_m = 0.41$ mm/s and $W_s = 0.36$ mm/s, respectively. The Mössbauer parameters of the broad sextet (δ_m, Δ_m, B_m, W_m) with a relative intensity of 25 % can be grossly associated with the α-Fe phase in agreement with the characteristic XRD patterns of the A533B samples. The Mössbauer parameters of the broad singlet with relative intensity of 75 % can be associated with the γ-Fe phase, as will be discussed next.

3.2.2 Mössbauer spectrum of the AISI-316 stainless steel

The transmission Mössbauer spectrum of AISI-316 stainless steel consists of a broad singlet whose hyperfine parameters are: $\delta_{AISI-316} = -0.098(2)$ mms^{-1}/α-Fe and a line width $W_{AISI-316} = 0.48$ mm/s, its isomer shift being characteristic for the γ-Fe phase in agreement with the XRD pattern, Fig. 1a. As observed, the values of δ_s and $\delta_{AISI-316}$ are very close to each other, suggesting the same iron phase in both stainless steels, i.e., the γ-Fe phase. The minor differences between these isomer shifts should be associated with the effect of the different alloying elements between these stainless steels and statistical errors.

On the other hand, the absence of the XRD pattern of the γ-Fe phase in the A533B stainless steel samples would suggest that the presence of the broad CXMS singlet, already assumed to be due to γ-Fe phase, arises from a thin film of the A533B steel samples. XRD runs longer than the present ones should be carried out in order to see whether the γ-Fe phase appears or not. This matter will be settled in the near future.

3.2.3 Numerical handling of the Mössbauer data

A careful analysis of the CXMS spectra of the A533B samples, composed of the magnetic (δ_m, Δ_m, B_m, W_m) and singlet (δ_s, W_s) patterns, Fig. 1b, indicated, however, that either the broad sextet or the broad singlet can be decomposed in more than one pattern each. Whereas the sextet could be fitted with two sextets with hyperfine magnetic fields and relative intensities of 33 (18.8 %) and 30.5T (9.6 %), the singlet could be fitted with a singlet ($\delta_1 = -0.110(2)$ mms^{-1}/α-Fe, $I_1 = 15.7$ %) and a quadrupole doublet ($\delta_2 = -0.109(2)$ mms^{-1}/α-Fe, $\Delta_2 = 0.18$ mm/s, $I_2 = 55.9$ %). While the sextet with $B = 33$ T can be attributed to iron atoms in the unperturbed iron matrix, i.e., the pure or unperturbed α-Fe phase, the sextet with $B = 30.5$ T can be attributed to iron atoms surrounded in their first or second neighbor shells by alloying elements (the 'perturbed' component) [4–7].

Because of the high relative intensity of the broad singlet in the CXMS spectra (>70 %), it was decided to analyze the changes in it while applying heat treatments to the A533B samples as described in the experimental section. Thus the CXMS spectra, recorded with a velocity close to 2 mm/s, will be analyzed using discrete value calculations (DVC's) and hyperfine distribution calculations (HDC's) of the hyperfine parameters, involving a singlet
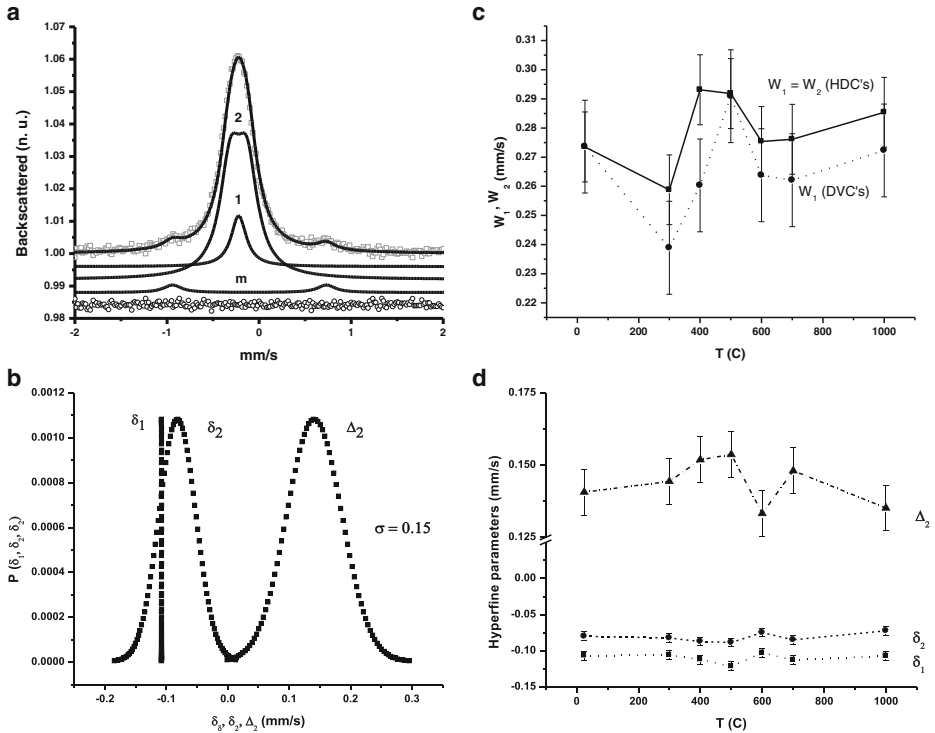
Fig. 2 a Characteristic CXMS spectrum of the A533B stainless steel obtained with a reduced velocity and fitted by using a singlet (W_1, δ_1) and two doublets (W_m, δ_m, Δ_m and W_2, δ_2, Δ_2), where W's stand for the line width; **b** Characteristic hyperfine distributions of the hyperfine Mössbauer parameters of the singlet with δ_1 and quadrupole doublet with δ_2, Δ_2 are depicted in this figure. The maxima values for δ_1 and δ_2 are referred to the isomer shift of metallic iron ($\delta_{\alpha-Fe} = -0.114$ mm/s). **c** Temperature dependence on the line width of the singlet (W_1). The line widths of the doublet (W_2) remained practically constant if calculated separately. **d** Temperature dependence of the hyperfine parameters of the singlet (δ_1) and quadrupole doublet (δ_2, Δ_2) obtained from the maxima of the Gaussian distribution functions

and two doublets. Figure 2a shows a typical result using DVC's, as explained next. However, let us first consult Table 1 which shows the typical least squares fitting result while calculating the hyperfine parameters and the relative intensities of the broad singlet and the resulting internal magnetic doublet associated with the broad sextet while using DVC's. Under these low velocity conditions ($\sim$2 mm/s), the singlet pattern is practically alone and only a small contribution ($\sim$4.38 %), associated with the inner magnetic doublet of the perturbed and unperturbed α-Fe phase is present. The hyperfine parameters describing this inner magnetic doublet (δ_m, Δ_m) were calculated as average values of its center, defined as δ_m (mm/s) = (line 1 position + line 2 position)/2 and its line separation by Δ_m.(mm/s) = line 2 position – line 1 position; the line widths were assumed to be equal and the calculated value was $W_m \approx 0.35$ mm/s.

Thus, Fig. 2a shows a typical DVC's result when the broad singlet is decomposed into a singlet and a quadrupole doublet. Unique solutions for the relative intensities of the singlet (δ_1, W_1) and quadrupole doublet, (δ_2, Δ_2, W_2), could not, however, be obtained when using DVC's. That is, by changing the starting intensity values of these patterns a little, the relative intensity of the singlet may be higher than that of the doublet, and vice versa.

Table 1 Mössbauer parameters of the singlet and inner magnetic doublet of the heat treated A533B samples using DVC's

T(C)	δ_1 (mm/s)[1]	$I_1(\%)$	δ_m (mm/s)[3]	Δ_m (mm/s)[4]	$I_m(\%)$
25	−0.111	96.76	−0.006	1.779	3.24
300	−0.111	94.46	−0.005	1.726	5.54
400	−0.118	96.54	−0.019	1.773	3.46
500	−0.125	96.28	−0.015	1.796	3.72
600	−0.117	93.44	−0.017	1.733	6.56
700	−0.113	94.74	−0.015	1.753	5.26
1000	−0.111	94.01	0.005	1.765	2.90
Av. Va.	−0.115	95.18[2]	−0.011	1.761	4.38[5]
	[1](±0.001);	[2](±0.54);	[3](±0.001);	[4](±0.023);	[5](±0.51)

Because of this, these parameters were estimated by using multiple hyperfine distribution calculations (HDC's) instead. Thus, the distribution functions for the isomer shift of the singlet (δ_1) and those of the isomer shift and quadrupole splitting of the quadrupole doublet (δ_2, Δ_2) were obtained by using a home-made computing program based on a Levenberg-Marquard routine. The inner magnetic doublet was simultaneously calculated using DVC's. Figure 2b shows the resulting Gaussian shaped distributions of the hyperfine parameters for the untreated sample. The same Lorentzian line width for the singlet (δ_1, W_1) and doublet (δ_2, Δ_2, W_1) was used; the results are shown in Fig. 2c. The obtained maxima of the three Gaussian distributions (δ_1, δ_2, Δ_2) as a function of temperature are shown in Fig. 2d. The line width W_1 showed slight temperature dependence as shown in Fig. 2c. While using HDC's a unique solution was obtained in relation to the relative intensities of the distributions involved. That is, Fig. 2b shows a typical result where the areas of the associated distributions for δ_2 and Δ_2 are always greater than the one associated with δ_1.

Thus results described in Fig. 2b, c and d were obtained by considering the presence of the inner magnetic doublet (with parameters δ_m, Δ_m, W_m), as shown in Table 1, using HDC's. A similar numerical analysis was carried out without considering this magnetic doublet and the results were essentially the same as those shown in Fig. 2b, c and d. This similarity did not occur, however, when the DVC's were carried out. For example, when the inner magnetic doublet is ignored, the isomer shifts of the singlet (δ_1) and quadrupole doublet (δ_2) are practically the same, suggesting similar electron densities at the ^{57}Fe nuclei, which may not be real. In addition to this, a minimum for I_1 and a maximum for I_2 appear at 500 °C, and $I_1 > I_2$, as shown in Fig. 3a. Marked minima for the isomer shifts (δ_1, δ_2) and quadrupole splitting (Δ_2) occur at 500 °C (not shown), which may also be unrealistic. If the inner magnetic doublet is included in the DVC analysis, the minimum and maximum for I_1 and I_2, (Fig. 3a), practically disappear and now $I_2 > I_1$, see Fig. 3b, in agreement with the HDC's as shown in Fig. 2b. That is, when using DVC's on these spectra, a multi solution for the hyperfine parameters and relative intensities is obtained and more than one defect is suggested from the variations of the quadrupole splitting. This does not occur while analyzing the same spectra using HDC's, even when the magnetic doublet of low relative intensity ($I_m \approx 4.38$ %) is or is not included in the analysis, Fig. 2d. Thus the obtained relative intensities from the DVC's, Fig. 3b may represent the actual situation which is in agreement with the HDC's (Fig. 2b).
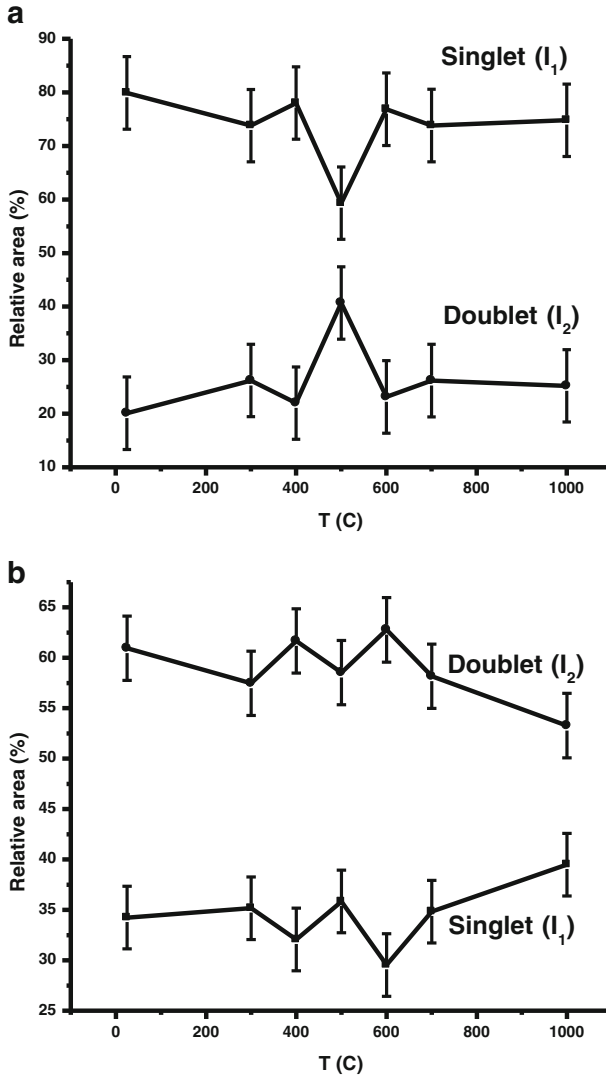
Fig. 3 Temperature dependences of the relative areas of the singlet and quadrupole double **a** without considering the magnetic doublet with parameters: W_m, δ_m, Δ_m, and **b** considering this magnetic doublet

4 Discussions

4.1 The thin film origin

According to the present XRD analysis, the A533B stainless steel crystallizes in the α-Fe phase only. From the CXMS spectra of these stainless steel samples two iron phases appear, however. A broad magnetic sextet characteristic of unperturbed and perturbed α-Fe phases is clearly suggested. A broad singlet arising from the surface of the A533B samples may be associated with the γ-Fe phase or an unknown iron compound. This singlet was unexpected

in the CXMS spectrum of the A533B samples. Longer XRD runs on the A533B samples are, however, required to asses this thin film idea properly; low temperature Mössbauer measurements are also required. The presence of such a thin film was already present in the untreated samples. Its origin was not thoroughly investigated although it probably arose as an effect of the machining process of the samples during their preparation. The presence of a similar and unexpected thin film was also observed in an S3A soft magnetic alloy, after being exposed to nitrogen plasma under temperatures not higher than 300 °C [8]. Particularly, the γ-Fe phase is a high temperature phase [9] and in both cases, i.e., the untreated A533B and S3A samples were not subject to any high temperature treatment to explain the presence of such a phase. In this sense the presence of the broad singlet in the CXMS spectra of these materials remains unclear.

4.2 The singlet (δ_1, W_1)

The CXMS singlet, Fig. 2a, with parameters W_1 and δ_1, described in Fig. 2c and d, can unambiguously be assigned to an approximate cubic symmetry around the iron sites. The resulting average isomer shift ($\delta_1 = -0.110(6)$ mms^{-1}/α-Fe), derived form HDC's, Fig. 2d, is practically the same as that obtained with DVC's, i.e., $\delta_{A533B} = -0.115(4)$ mms^{-1}/α-Fe. The latter value was obtained by ignoring the presence of the superimposed quadrupole doublet with parameters δ_2, Δ_2. The latter values of (δ_1 and δ_{A533B} approach those reported by different authors [8, 9]. For instance, the corresponding isomer shift of the broad CXMS singlet for 4140 stainless steel, which crystallizes in both the α-Fe and γ-Fe phases, is $\delta_{4140} = -0.110(2)$ mms^{-1}/α-Fe [8]. On the other hand, the isomer shift of the characteristic broad CXMS singlet of the AISI-316 stainless steel, which crystallizes in the γ-Fe phase only, Fig. 1a, is $\delta_{AISI-316} = -0.098(2)$ mms^{-1}/α-Fe. Under these considerations, the singlet arising from the surface of the A533B steel may also arise from the γ-Fe phase. More research is, however, required to define the nature of this CXMS singlet of the A533B steel. In addition to these data, a broad singlet also appears in the CXMS spectrum of the S3A soft magnetic alloy, exposed to a nitrogen plasma, with $\delta_{S3A} = -0.110(4)$ mms^{-1}/α-Fe; this also is associated with the γ-Fe phase [8]. HDC's are required on the CXMS singlets of these AISI-316 and 4140 S3A metals to characterize them properly. Macedo and Keune [9] also studied broad CXMS singlets arising from 10 and 17 mono-layers (10-ML, 17-ML) samples of γ-Fe(100) films, pseudo-morphically grown on Cu(100) surfaces under UHV conditions [9]. These broad singlets were analyzed in terms of a singlet and a quadrupole doublet as well [9], as in the present paper. The corresponding isomer shifts of these singlets for these samples are $\delta_{10-ML} = -0.077(5)$ and $\delta_{17-ML} = -0.085(3)$ mms^{-1}/α-Fe, respectively [9]. In Macedo and Keune's study the quadrupole doublet appears with a relative intensity lower than that of the singlet; the parameters of this doublet are $\delta_{17-ML} = +0.02(2)$ mms^{-1}/α-Fe and $\Delta_{17-ML} = 0.57(5)$ mm/s and is attributed to asymmetric sites around the Fe atoms which are surrounded by a certain number of neighboring Cu atoms, all of which are located at the Fe-Cu interface [9]. One may note that the hyperfine parameters of this quadrupole doublet differ from those here obtained, i.e., the isomer shift ($\delta_{17-ML} = +0.02(2)$ mms^{-1}) and the quadrupole splitting ($\Delta_{17-ML} = 0.57(5)$ mm/s) are higher than those for A533B: $\delta_2 = -0.081(6)$ mms^{-1} and $\Delta_2 = 0.143(7)$. Such a difference clearly arises from the nature of the samples and the formation process between these thin films.

4.3 The superimposed quadrupole doublet (δ_2, Δ_2, W_2)

On the other hand, this quadrupole doublet of relative intensity higher than that of the singlet with average hyperfine parameters $\delta_2 = -0.081(6)$ /α-Fe and $\Delta_2 = 0.143(7)$ mms^{-1} may be attributed to slightly asymmetric sites around the iron atoms. Several possibilities may be considered to explain this doublet. Interstitials may produce this asymmetry; random iron substitutions by different atoms are other possibilities; the presence of mono- or multi-vacancies close to the iron sites is a third possibility. In order to choose among these possibilities, let us first assume that the Mössbauer fraction for these iron sites is the same. Since the relative intensity of the quadrupole doublet is higher than that of the singlet, this fact would then suggest that this thin film is highly defected. On the other hand, the relative content of the constituting atoms different from iron accounts for 3.204 % only, as can be checked from the elemental composition data given in the experimental section. This may suggest that atomic substitution and/or the presence of interstitials may not produce such a large intensity of the quadrupole doublet. This atomic elimination would suggest as the main motive that could explain the presence of the quadrupole doublet the mono- or multi-vacancies. The small magnitude of the quadrupole splitting of the doublet, $\Delta_2 = 0.143(7)$ mm/s, Fig. 2d) suggests the presence of a small lattice distortion around the iron sites. This small distortion would be produced by mono-vacancies rather than multi-vacancies, the latter producing a quadrupole splitting which would be higher than the measured one. In this context the presence of mono-vacancies are suggested to explain this quadrupole doublet with average hyperfine parameters $\delta_2 = -0.081(6)$ mms^{-1}/α-Fe and $\Delta_2 = 0.143(7)$ mms^{-1}/α-Fe, and is adopted here; this may be supported by other papers [10–12].

4.4 The line widths W_1 and W_2

The line widths of the singlet (with parameter δ_1) and of the doublet (with parameters δ_2, Δ_2) were assumed to be equal and their variations with temperature is as shown in Fig. 2c. When these line widths were calculated independently of each other, the line width of the doublet remained constant and the variation of W_1 vs T is also shown in Fig. 2c. Generally, there is a small variation of these line widths with temperature. In both cases, however, W_1 and W_2 are higher than the natural line width ($W_N = 0.194$ mm/s), Fig. 2c. Such a broadening can be associated with: (a) a heterogeneous atomic surrounding around the ^{57}Fe sites due to the multi-elemental composition of the A533B stainless steel, as already mentioned and also suggested by the variations of the hyperfine parameters δ_1, δ_2 in Fig. 2d; (b) tiny lattice distortions at the ^{57}Fe sites due to the presence of different atomic substitutions at lattice points of atoms other than Fe, as represented by the variation of Δ_2 in Fig. 2d [8]. According to the DVC's and including the magnetic doublet, the relative amount of the singlet with I_1 ranged from 32 to 43 %, depending on the heat treatment, Fig. 3b. The quadrupole doublet with I_2, as shown in Fig. 3b, contributes with a relative intensity higher than that of the singlet ranging from 57 to 68 % depending on the heat treatment. That is I_2 is always higher than I_1. If the magnetic doublet is ignored in the DVC analysis, these relative intensities are reversed, Fig. 3a, i.e., $I_1 > I_2$. The former case has therefore been taken as the representative one.

According to the above discussion, the best fit analysis was obtained when using HDC's, whether or not the inner magnetic doublet arising from the α-Fe phase is included. This analysis also suggested that there was no a marked temperature dependence on the hyperfine parameters. Particularly, the quadrupole splitting parameter was the most affected and from

this, one might infer the presence of at least two defects. The standard deviation of these measurements indicated to us, however, that such variations with temperature were within the statistical error, and because of this only a single defect is suggested, consisting of the presence of monovacancias, as already discussed. The number of these defects practically remained constant, within experimental error, after the thermal treatments as indicated in Fig. 3b.

5 Conclusions

The surface of heat treated A533B stainless steel samples was studied using XRD and CXMS techniques. The XRD patterns of the untreated and treated A533B samples showed a single phase, the α-Fe phase. On the other hand, the conversion X-ray Mössbauer spectrum of the stainless steel samples consisted of a broad singlet which may be characteristic of the γ-Fe phase or an unknown iron compound, arising from a thin film of the stainless steel samples as a result of the machining process during their preparation, and a broad sextet characteristic of the unperturbed and perturbed α-Fe phase. The broad CXMS singlet of the A533B samples was further decomposed into a singlet and a quadrupole doublet. While the former might be associated with a defect free γ-Fe phase having a slightly distorted fcc atomic structure due to iron substitutions and interstitials from the alloying elements, the quadrupole doublet was associated with point defects in this γ-Fe phase, where monovacancies may be involved, whose amount remained constant throughout the present heat treatments.

References

1. Van Black, L.H.: Elements of Materials Science and Engineering, 3rd edn. Addison-Wisley (1975)
2. Abdel-Hady, E.E.: Nucl. Inst. Method Phys. Res. B **221**, 225–229 (2004)
3. Bibicu, I., Rogalski, M.S., Nicolescu, G.: Meas. Sci. Technol. **7**, 113–115 (1996)
4. de Bakker, P.M.A., Slugen, V., De Grave, E., van Walle, E., Fabry, A.: Hyperfine Interact. **110**(11), 11–16 (1997)
5. Slugeň, V., Lipka, J., Hasčík, J., Gröne, R., Tóth, I., Uváčik, P.A., Zeman, A., Vitázek, K., Mashlan, M., et al. (eds.): Material Research in Atomic Scale by Mössbauer Spectroscopy, pp. 187–198. Kluwer Academic Publishers (2003)
6. Brauer, G., Matz, W., Fetzer, Cs.: Hyperfine Interact. **56**, 1563–1568 (1990)
7. Idczak n, R., Konieczny, R., Chojcan, J.: Solid State Commun. **152**, 1924–1928 (2012)
8. Cabral-Prieto, A., Nava, N., García-Sosa, I., Camps, E., Escobar, L., López-Castañares, R., Oleacardoso, O.: J. Mater Sci. Eng. **1**(5), 632-638 (2011)
9. Macedo, Q.A.A., Keune, W.: Phys. Rev. Lett. **61**(4), 475–478 (1988)
10. Collins, G.S., Peng, L.S.J.: Il Nuovo Cimento **18D**(329), 1–9 (1996)
11. Lipka, J.: Jordan J. Phys. **2**(2), 73–8 (2009)
12. Chojcan, J.: Acta Phys. Pol. A **100**(5), 723–729 (2001)